Scalable Photonic-Assisted Multipath Self-Interference Cancellation Based on Optical Frequency Comb

Zhe Liu, Dayong Wang, Jing Zhang, Jinchuan Yao, Yunxin Wang, Yuanfen Zhou, and Lu Rong

***Abstract*—In order to increase the scalability and reduce the complexity of photonic multipath SIC systems, a photonic multipath self-interference cancellation (SIC) method based on optical frequency comb (OFC) is proposed. The OFC is generated by continuously frequency-shifting the seed laser in the re-circulating frequency shifter (RFS) loop. The reference signal is modulated to the multiple combs of the OFC via a Mach-Zehnder modulator (MZM), and the received signal is loaded into another MZM. These two MZMs work at opposite quadrature bias points to reverse the phase of the received signal and the reference signal. After splitting and filtering with a dense wavelength division multiplexer, the reference modulation signals are injected into a multipath amplitude-delay matched link, where the amplitude and delay time are accurately controlled by several sets of optical variable attenuators and tunable delay lines. Both the inversion and amplitude-delay matching of the reference signals are realised in the optical domain, contributing to a broad bandwidth and high operational frequency. Experimental results show that the cancellation depth is greater than 45.9 dB for single-frequency signals, and 23.9 dB for signals with a bandwidth of 100 MHz in a setup with three self-interference paths. The proposed method is characterized by easy scalability, good flexibility, and low cost, making it suitable for complex multipath SIC in in-band full-duplex wireless systems.**

***Index Terms*—In-band full duplex, re-circulating frequency shifter, optical frequency comb, multipath self-interference cancellation.**

I. Introduction

WIDEBAND in-band full-duplex (IBFD) wireless systems have found a diverse range of applications in new-generation mobile communications, satellite communications, radar communications, etc. In IBFD technology, signals are sent and received simultaneously at the same carrier frequency, which can greatly improve the spectrum utilisation through doubling of the data rate. However, IBFD also suffers from serious self-interference (SI) problems. Microwave photonics technology has attracted widespread attention owing to its large bandwidth, low loss, and resistance to electromagnetic interference [1], [2], [3], and this technology has been used for SI cancellation (SIC), as it gives the SIC a larger operating bandwidth and more accurate phase matching compared with the SIC in the electrical domain [4]. SI signals are generated by leakage between antennas or reflection from external obstacles. At higher power, SI signals generally submerge the signal of interest (SOI), leading to deterioration of the system sensitivity and dynamic range. In order to achieve SIC, the transmitting signal is split through a power divider to provide a reference signal (SR), which is then adjusted to give an equal amplitude and a reverse phase to the SI. In recent years, a variety of RF SIC methods based on microwave photonics have been proposed. Delay adjustment can be achieved through the use of optical tunable delay lines (OTDL) [5], [6], fibre Bragg gratings (FBG) [7], [8], or dispersive elements (DE) [9], whereas amplitude adjustment can be implemented with optical variable attenuators (OVA) [10] or semiconductor optical amplifiers (SOA) [11]. The inversion of the SI and SR signals can be realised by an electric phase shifter (EPS) [12], a balanced detector (BPD) [13], [14] and an RF Balun transformer [15]. In these methods, the phase inversion is implemented in the electrical domain, leading to a limited SIC cancellation depth and bandwidth. To extend the bandwidth and regulate the phase more precisely, several phase inversion methods have been investigated in the optical domain, for example using a dual phase modulator (PM) [16], dual Mach-Zehnder modulator (MZM) [17], dual-parallel MZM (DP-MZM) [18] or dual-parallel polarization modulators (DP-PolM) [19]. These solutions have been demonstrated to be effective for a single-path SIC, but they are not suitable for a multipath SIC.

In practical applications, multiple obstacles are commonly encountered along the transmitting path from the transmitting antenna. This means that multiple self-interfering signals will be detected by the receiving antenna, resulting in a complex multipath SI problem. In complex IBFD multiple-input multiple-output (MIMO) systems, in addition to the SI signals described above, co-site multipath SI becomes an issue, which is caused by the reflection of multiple local transmitting signals. Single-path SIC approaches cannot effectively suppress multiple SI signals. In order to solve the multipath SIC problem, a series of

Manuscript received 15 February 2024; accepted 19 February 2024. Date of publication 26 February 2024; date of current version 7 March 2024. This work was supported by the National Natural Science Foundation of China under Grant 62275008 and Grant 62220106005. *(Corresponding author: Yunxin Wang.)*

The authors are with the School of Physics and Optoelectronic Engineering, Beijing University of Technology, Beijing 100124, China, and also with the Beijing Engineering Research Center of Precision Measurement Technology and Instruments, Beijing University of Technology, Beijing 100124, China (e-mail: 451125346@qq.com; wdyong@bjut.edu.cn; zhangjing@bjut.edu.cn; 1411931655@qq.com; yxwang@bjut.edu.cn; zhouyuanfen222@163.com; ronglu@bjut.edu.cn).

Digital Object Identifier 10.1109/JPHOT.2024.3369669

incoherent SR signals must be introduced, and the number of SR signals should match the number of interfering paths. Therefore, the key to multi-path SI cancellation lies in creating multiple incoherent SR signals. Several multipath SIC schemes based on multiple tunable lasers or single-frequency lasers have been proposed. In [9], a PolM and a polarizer were combined to reverse the SR signal, and delay matching was accomplished by tuning the wavelength to change the time delay after passing through a DE. This method achieved a two-path cancellation depth of 44 dB over a bandwidth of 50 MHz. However, several costly tunable lasers were required, and the accuracy of the delay matching was determined by the tunability accuracy of the laser. In [20], multipath SIC was realised by multiple lasers and PMs, with a cancellation depth of more than 26 dB for a two-path bandwith of 100 MHz. However, single sideband modulation was realised with an optical processor, meaning that the lowest operational frequency of the RF signal was limited by the slope edge of the optical filter. Recently, a new photonics-assisted multipath SIC method based on a dual-MZM structure was proposed for wideband IBFD MIMO radio-over-fibre (ROF) transmission systems [21]. Experimental results showed that cancellation depths of 30.18, 24.9, 22.7 and 20.88 dB could be achieved with bandwidths 100 MHz, 500 MHz, 1 GHz and 2 GHz, respectively. In the methods described above, the number of lasers determines the number of SI paths that can be cancelled, and as the number of SI paths increases, the system complexity and cost will increase significantly. In view of this, a laser sharing scheme based on a single-mode to multimode (SM-MM) coupler has also been proposed [10], [22]. Since SM-MM couplers make the spatial modes of the different input signals almost orthogonal to each other [23], several SRs do not mutually interfere in a multi-mode photodetector (PD), thus enabling multipath SIC. In [10], phase inversion of the SR was achieved by a polarisation controller (PC) and polariser, and this approach featured a large operation bandwidth. The scalability of this scheme was limited by the number of orthogonal spatial modes that could be multiplexed by the SM-MM coupler. However, this element relies on a coupling lens system, and its structure will grow more complex as the number of inputs increases [24]. Furthermore, to simplify multipath systems, several digitally assisted multi-path SIC methods have been proposed based on a least square (LS) algorithm [25], recursive least square (RLS) algorithm [26], [27], and least mean square (LMS) algorithm [28] *etc*. These methods require an additional transmitter system for digitally generating the reference signals. The algorithms adaptively adjust the delay and amplitude of the multiple reference signals. However, the bandwidth of digitally-assisted multi-path SIC systems is limited by electrical devices, particularly the digital-to-analog converters (DACs).

Optical frequency comb (OFC) lasers have received significant research interest owing to the high stability of the frequency and phase between the combs. OFCs have been widely used in the fields of distance measurement [29], [30], microwave photonic channelised receivers [31], [32], frequency measurement [33], etc. When OFCs are combined with multipath SIC, the need for multiple discrete lasers can be avoided, and the complexity and cost of the system are both reduced. OFCs can be generated by many schemes, such as micro-ring resonant cavities [34], mode-locked lasers [35], electro-optical modulators [36], four-wave mixing [37], and re-circulating frequency shifters (RFS) [38]. In the RFS method, an OFC is generated by constantly shifting the frequency of the seed laser in the loop through carrier-suppressed single-sideband (CS-SSB) modulation. This method has the advantages of a simple structure, a high number of combs, precise control over the number of combs, and fine flatness. All of these factors can improve the scalability and stability of the system. It is worth mentioning that high-order comb noise floor will rise due to the accumulation of ASE noise when the RFS loop outputs a large number of combs, which can be effectively solved by a finite impulse response (FIR) filter [39].

In this paper, we propose and demonstrate a photonics-assisted multipath SIC method based on an OFC. The OFC is generated by continuous frequency-shifting and CS-SSB modulation in the RFS loop. The combs are used as optical carriers for the multiple reference signals. Inversion of the reference signals is achieved by using dual-MZM modulators, after which the SR signals are split via a dense wavelength division multiplexer (DWDM). Several sets of OVAs and OTDLs are used to precisely control the amplitude and delay of the SR signal to satisfy the cancellation conditions. The received signal and the SR signal are coupled by another DWDM, and the SOI can be recovered after frequency beating at the PD. Experimental results demonstrate the capability of multipath SIC and signal recovery. It is easy to increase the number of optical carriers output from the RFS-OFC, meaning that the system avoids the need for multiple discrete lasers and has good scalability; meanwhile, the number of optical carriers can be changed by adjusting the bandwidth of the optical bandpass filter in the RFS loop, enhancing the system's flexibility and compactness.

II. Rinciple

A schematic of the proposed scheme is shown in Fig. 1(a). The optical carrier output from a laser diode (LD) is divided into two beams through an optical coupler (OC): one is fed to MZM1 for modulation of the received signal, and the other is injected into the RFS loop to generate an OFC. The received signal contains the SOI and the SI signal. The SR is modulated to the OFC through MZM2. To accomplish the inversion of the SI and SR signals, MZM1 and MZM2 operate at the positive and negative slope quadrature bias points, respectively. The OFC is demultiplexed by DWDM1. The number of DWDM channels is no less than the number of SI paths. The amplitude and delay of the SR for each path are then adjusted through the use of an OVA and an OTDL. Following this, another DWDM is used to combine all the paths, and multipath SI cancellation can be implemented after frequency beating at the PD.

The transmitting signal is split through a power divider to produce the SR. The SR signal S_{SR} and the SI signal S_{SI} can be expressed as

$$\begin{cases} S_{SR}(t) = \alpha_{SR} V_{RF} \cos(\omega_{RF} t) \\ S_{SI}(t) = \sum_{n=1}^{N} S_n(t) = \sum_{n=1}^{N} \alpha_n V_{RF} \cos[\omega_{RF}(t+\tau_n)] \end{cases} \tag{1}$$

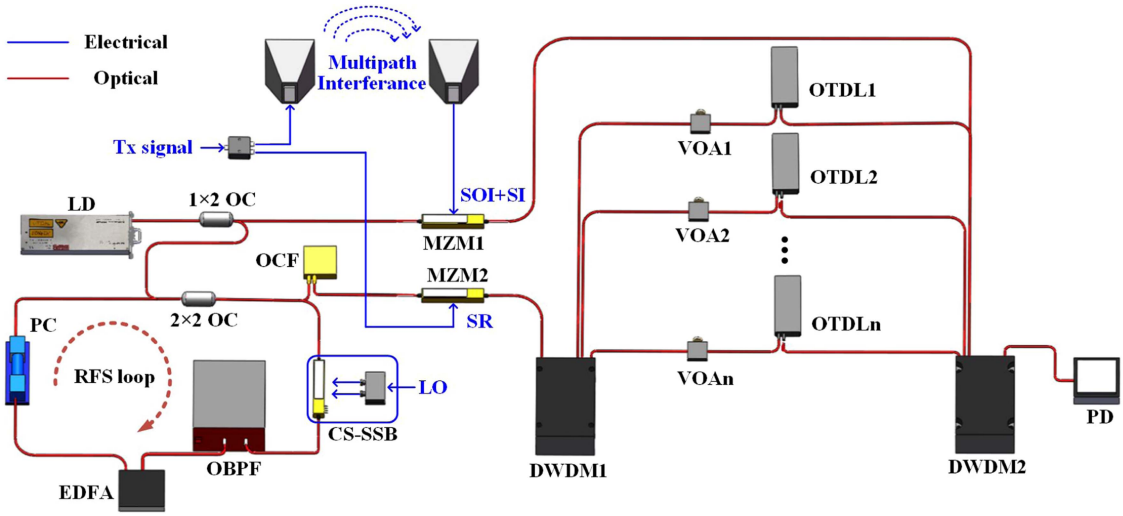

Fig. 1. Schematic diagram of the proposed method. LD: laser diode; MZM: Mach-Zehnder modulator; SR: signal of reference; SOI: signal of interest; SI: self-interference signal; LO: local oscillator signal; OC: optical coupler; OBPF: optical bandpass filter; OCF: optical comb filter; PD: photodetector; PC: polarisation controller; EDFA: Erbium-doped fibre amplifier; CS-SSB: carrier-suppressed single-sideband; DWDM: dense wavelength division multiplexing; OTDL: optical tunable delay line; OVA: optical variable attenuator.

where V_{RF} and ω_{RF} are the amplitude and angular frequency of the transmitting RF signal, α_{SR} is the attenuation coefficient of the power divider, S_n is the SI signal in the n^{th} path, N is the number of self-interfering paths, and α_n and τ_n are the attenuation coefficient and delay time of the SI signal, in the n^{th} path, respectively.

The optical carrier is split into two arms, one of which is used to modulate the received signal, and the other to supply the seed laser for the RFS loop. In order to simplify the analysis below, the SOI signal is removed to clearly show the cancellation process. Thus, only the SI signal modulates MZM1, which works at the positive slope orthogonal bias point. After expansion using the Jacobi-Anger formula and ignoring small signals, the output of the MZM1 can be written as

$$E_{SI-MZM1}(t) \propto E_0 e^{j\omega_c t}\left[e^{j\pi\left(\frac{S_{SI}(t)}{V_\pi}-\frac{1}{2}\right)}+e^{j\pi\left(-\frac{S_{SI}(t)}{V_\pi}\right)}\right]$$

$$\propto \sum_{n=1}^{N} E_0 e^{j\omega_c t} e^{-j\frac{\pi}{4}}\begin{bmatrix}1+J_1(m_0\alpha_n)\,e^{j\omega_{RF}(t+\tau_n)}\\ +J_1(m_0\alpha_n)\,e^{-j\omega_{RF}(t+\tau_n)}\end{bmatrix} \quad (2)$$

where E_0 and ω_c are the amplitude and angular frequency of the optical carrier input to MZM1, and $m_0 = \pi V_{RF}/V_\pi$ is the modulation depth, where V_π is the half-wave voltage.

The seed laser is fed to the RFS loop, and CS-SSB modulation produces a frequency shift of ω_{LO} for each cycle, so the RFS output after the 1st loop can be expressed as

$$E_1(t) \propto E_0 e^{j\omega_c t} + l_0 g_0 E_0 e^{j(\omega_c+\omega_{LO})t} \quad (3)$$

where l_0 is the loss factor of the RFS loop, and g_0 is the gain coefficient of the EDFA.

After the M^{th} loop, the output can be expressed as

$$E_M(t) \propto E_0 \sum_{n=0}^{M} l_0^n g_0^n e^{j\omega_n t} \quad (4)$$

where $\omega_n = \omega_c + n\omega_{LO}$. In order to output a flat OFC, the EDFA gain is adjusted to satisfy $l_0 g_0 = 1$. The number of combs in the OFC is $M+1$, which is determined by the optical bandpass filter (OBPF). M can be designed to be equal to the number of self-interfering paths, i.e., $M = N$.

The SR is then injected into MZM2, which operates at the negative slope orthogonal bias point. After small signal approximation, the output of MZM2 can be expressed as

$$E_{SR-MZM2}(t) \propto E_0 \sum_{n=0}^{N} e^{j\omega_n t}$$

$$\left[e^{j\pi\left(\frac{S_{SR}(t)}{V_\pi}+\frac{1}{2}\right)}+e^{j\pi\left(-\frac{S_{SR}(t)}{V_\pi}\right)}\right]$$

$$\propto \sum_{n=0}^{N} E_0 e^{j\omega_n t} e^{j\frac{\pi}{4}}\begin{bmatrix}1-J_1(\alpha_{SR}m_0)\,e^{j\omega_{RF}t}\\ -J_1(\alpha_{SR}m_0)\,e^{-j\omega_{RF}t}\end{bmatrix} \quad (5)$$

The reference optical signals for the different paths are divided by DWDM1. The amplitude and phase of the SR signals on different paths are adjusted by sets of OVAs and OTDLs, respectively, and after being combined by DWDM2, the output can be described as

$$E_{SR-MZM2}(t) \propto \sum_{n=1}^{N} {\alpha'}_n E_0 e^{j\omega_n t} e^{j\frac{\pi}{4}}$$

$$\begin{bmatrix}1-J_1(\alpha_{SR}m_0)\,e^{j\omega_{RF}(t+{\tau'}_n)}\\ -J_1(\alpha_{SR}m_0)\,e^{-j\omega_{RF}(t+{\tau'}_n)}\end{bmatrix} \quad (6)$$

where ${\alpha'}_n$ is the attenuation coefficient of the OVA and ${\tau'}_n$ is the delay of the OTDL for the n^{th} path.

It is worth noting that the carrier is filtered out after DWDM1, since this carrier has been utilised by the received RF signal. Finally, a PD is applied to complete the optical-electrical conversion. Neglecting the DC and higher order terms, the output

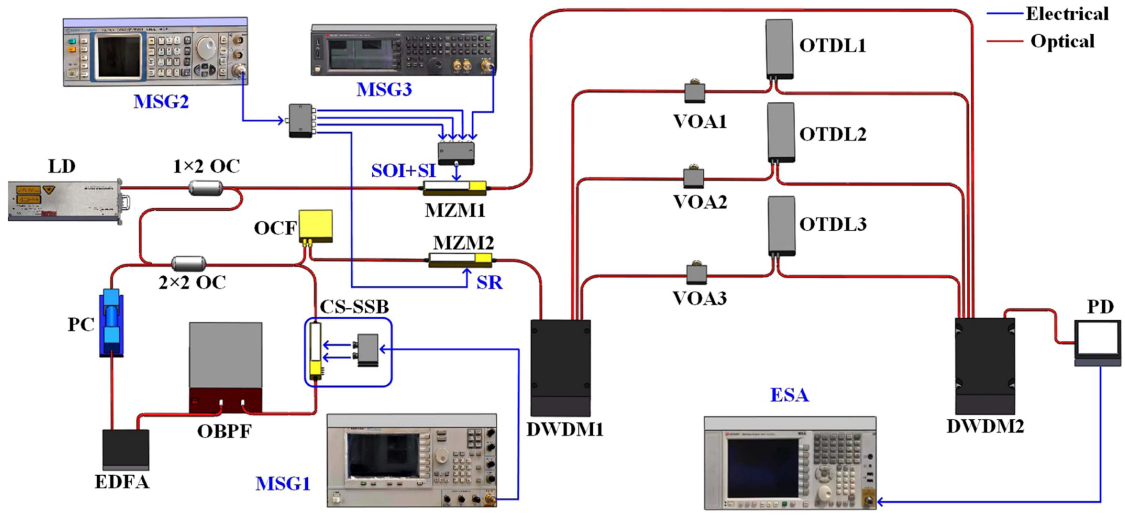

Fig. 2. Diagram of three-path self-interference cancellation experimental setup. MSG, microwave signal generator; ESA, electrical spectrum analyzer.

photocurrent can be denoted as

$$\begin{aligned} I_{PD}(t) &= \eta |E_{SI-MZM1}(t) + E_{SR-MZM2}(t)|^2 \\ &\propto \eta \sum_{n=1}^{N} E_0^2 J_0(m_0\alpha_n) J_1(m_0\alpha_n) \cos[\omega_{RF}(t+\tau_n)] \\ &- \sum_{n=1}^{N} \alpha_n'^2 E_0^2 J_0(\alpha_{SR} m_0) J_1(\alpha_{SR} m_0) \cos[\omega_{RF}(t+\tau'_n)] \end{aligned} \tag{7}$$

where η is the responsivity of the PD. From (7), it can be derived that the following conditions need to be satisfied for multipath SI cancellation

$$\begin{cases} \tau_n = \tau'_n \\ \alpha_n'^2 J_0(\alpha_{SR} m_0) J_1(\alpha_{SR} m_0) = J_0(m_0\alpha_n) J_1(m_0\alpha_n) \end{cases} \tag{8}$$

It can be seen that the phase deviation, tuning accuracy of the delay line and attenuator are three important factors affecting the cancellation performance in multipath SIC systems.

III. Experimental Result and Discussion

The feasibility and effectiveness of the proposed method was verified by building an experimental link as shown in Fig. 2. The optical carrier was output from the tunable laser (NKT Photonics) with an output centre wavelength of 1550.12 nm and power 14.2 dBm. After passing through a 1×2 OC, one arm was used as the reference light. The received signal (including SI and SOI) was loaded into MZM1, which operated at the positive slope quadrature bias point. The other arm went to the RFS link to generate the OFC, which was then loaded with a reference signal through MZM2. This modulator was adjusted at the negative slope quadrature operating point. A microwave signal generator (MSG1, Agilent E8257D) was used to produce an LO signal to drive the CS-SSB module in the RLS-OFC, and an OFC with a frequency spacing of LO frequency was generated. The transmitting signal generated by the MSG2 (Rohde & Schwarz SMB 100A) was split into four paths by a power splitter. One path formed the SR, and the other three were used as the SI signals. MSG3 (Rohde & Schwarz SMB 100A; Keysight N5182B) generates the SOI signal. The SI and SOI signals were combined through a power splitter and then loaded into MZM1 as the received signal. The OFC was input to MZM2 as a reference optical signal and output multipath SR after modulation via MZM2. The multipath SRs were split by DWDM1, and the amplitude and delay of the SI and SR signals were matched by adjusting the OTDLs and OVAs. After being combined by the DWDM2, all optical signals entered the PD (FINISAR, XPDV2120R, 50 GHz), and the output signal was measured by a spectrum analyzer (SA, Keysight N9020A). The OBPF (BVF-300CL) was applied to control the number of combs in the passband, while suppressing the out-of-band accumulated noise of the optical frequency comb. The maximum saturation output power of the EDFA was 22 dBm. In general, the bandwidths of commercial DWDMs are 25, 50, 100 GHz, etc., however, due to the limitations on the bandwidth of the LO source, it is difficult to generate OFCs with comb intervals greater than 40 GHz. Hence, the LO frequency had to be set to 25 GHz. When the RF frequency was low (<10 GHz), the OFC can be demultiplexed directly using a 25 GHz DWDM, as shown in Fig. 3(a). However, when the RF frequency is higher, the bandwidth of the optical reference signal of a single path will be greater than 25G, causing serious frequency mixing. To optimise the system bandwidth of the RF signal, we combined an OCF with a 50 GHz DWDM as shown in Fig. 3(b). The OCF is used to filter out half of the optical comb, changing the comb spacing to 50 GHz. Accordingly, the maximum bandwidth of the system was doubled. Simultaneously, the minimal work frequency was not constrained.

The OFC was then modulated by the SR and split into three reference signals by DWDM1, where the three channels of the DWDM had centre wavelengths of 1549.72, 1549.32, and 1548.92 nm, respectively. By using an OVA and an OTDL (MODL-300), the SR of each path was adjusted to ensure an

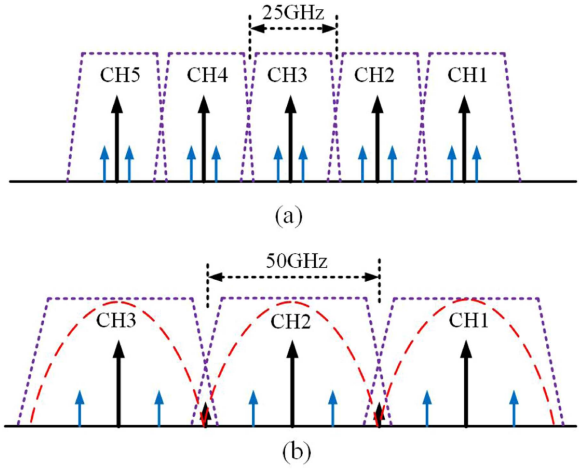

Fig. 3. Spectrograms diagram: (a) with a 25G DWDM and (b) with a 50G DWDM and an OCF.

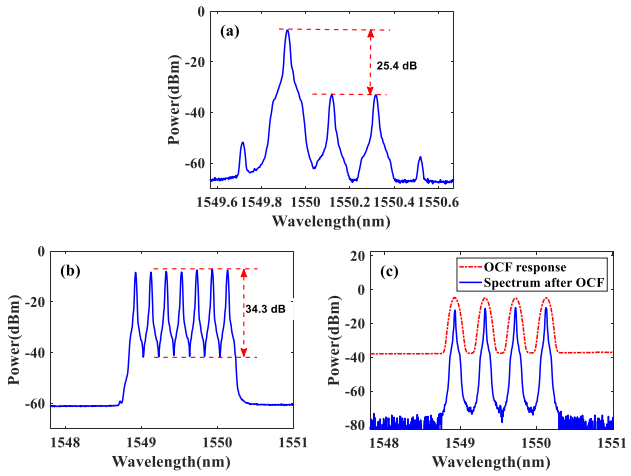

Fig. 4. Spectrograms: (a) output of carrier suppression single sideband module; (b) optical frequency comb; and (c) after the OCF.

equal amplitude and time delay as the SI signal of the corresponding path. The delay range and adjustment accuracy of the OTDL were 0–333 ps and 0.1 ps, respectively. The attenuation range of OVA in the experiment was 0.8–60 dB, and the adjustment accuracy was 0.02 dB. Finally, these three reference signals and the received signals were combined into a beam, and the multipath SI signals were eliminated after frequency beating in the PD.

A. Performance of the OFC

The OFC generated by the RFS link was measured using an optical spectrum analyser (Yokogawa, AQ6370C). The CS-SSB module was driven with a LO signal at 25 GHz. The output spectrum is shown in Fig. 4(a), and its spurious suppression ratio (SSR) reached 25.4 dB. By tuning the powers of the seed laser and the LO signal, the bandwidth of the OBPF was adjusted to retain the desired seven-comb OFC, and the output spectrum of the OFC is shown in Fig. 4(b). The average comb power was −8.1 dBm, and the effective optical SNR (OSNR) reached

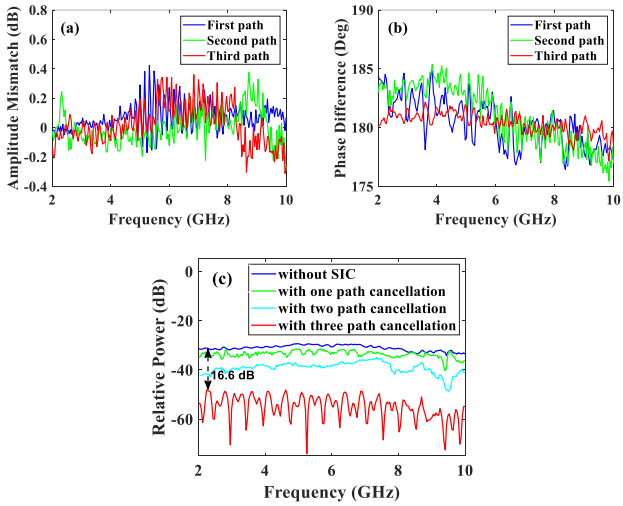

Fig. 5. (a) Amplitude match between the SR and SI paths; (b) Phase difference between the SR and SI paths; and (c) measured cancellation depth with and without SIC for a large bandwidth (2–10 GHz).

34.3 dB. In addition, these seven combs had a fine flatness of 1.9 dB. After the OCF, the OFC comb spacing was 50 GHz, and as shown in Fig. 4(c).

B. Performance of the Multipath SIC

In order to achieve optimal cancellation performance of the link, a vector network analyser (VNA, Rohde & Schwarz ZNB40) was used to adjust the reference paths one by one, to match the cancellation conditions. The scanning frequency range of the VNA was 2–10 GHz. After selecting a pair of SR and SI paths, the DC bias voltages of MZM1 and MZM2 were adjusted to maximize the system gain of the two paths, while maintaining a difference of about V_π in the DC bias voltages to achieve the inversion of SR and SI. Subsequently, the VNA was used to measure the time delay of the SR and SI paths separately. The length of the paths was adjusted to ensure that the time delay of each group of SRs and SIs was equal. Once each group of SR and SI paths had the same delay, the amplitude and phase difference between the SR path and the SI path were measured with the SI path as the reference. The OVA was adjusted to minimize the amplitude mismatch to near zero and the OTDL was adjusted to minimize the phase difference to near 180°.

The amplitude mismatch and phase difference after matching the three sets of paths are shown in Fig. 5(a) and (b), with a maximum deviation of 0.4 dB in amplitude and 5.4° in phase. After fine matching, the link was measured by using the VNA with and without the SR signal loaded, the results are shown in Fig. 5(c). It is observed that the cancellation depth is limited with only one path cancellation. With two-path cancellation, the average cancellation depth has improved from 2.6 dB to 8.1 dB. However, the cancellation capability is still limited for more SR paths exists. After three-path cancellation, the cancellation depth is more than 16.6 dB within the 8 GHz bandwidth.

The multipath cancellation effect was first verified using a single-frequency signal. In order to relax the analysis, the SOI

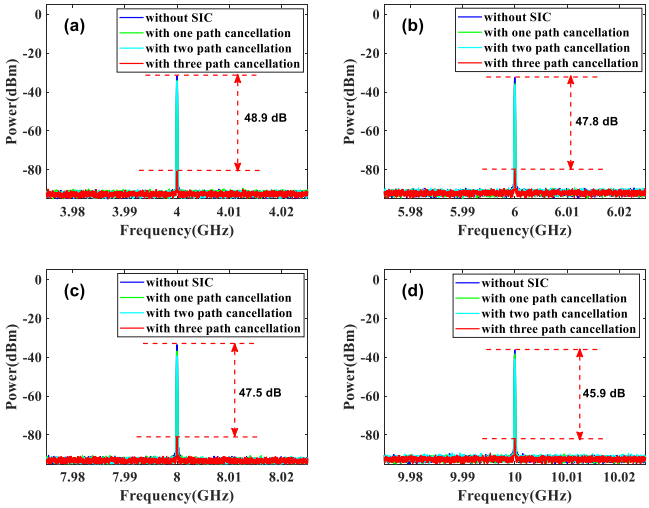

Fig. 6. Spectra after the PD, with and without SIC, for an SI with frequency (a) 4.0 GHz, (b) 6.0 GHz, (c) 8.0 GHz, and (d) 10.0 GHz.

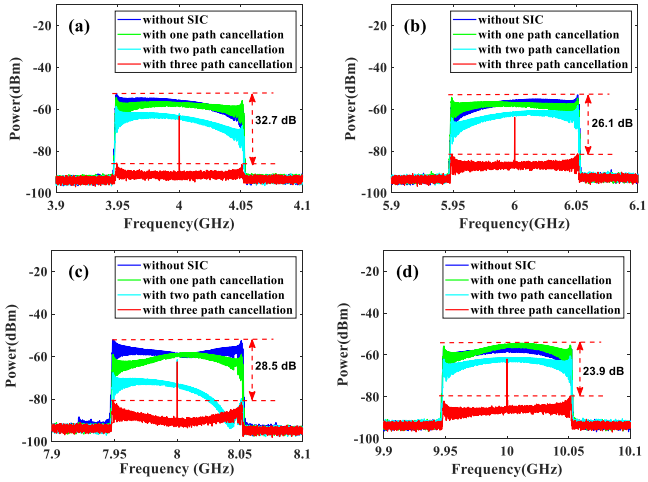

Fig. 7. Spectra after the PD, with and without SIC, when SI is a 100 MHz broadband signal with centre frequencies of (a) 4.0 GHz, (b) 6.0 GHz, (c) 8.0 GHz, and (d) 10.0 GHz.

signal was not loaded. The frequency of the microwave signals generated from the MSG was set to 4, 6, 8 and 10 GHz, and the resolution bandwidth (RBW) and video bandwidth (VBW) of the spectrometer were set to 100 kHz and 1 kHz, respectively. The measured output spectra are shown in Fig. 6. For the case where no SR was injected, the spectra without the SIC are shown as blue curves. For the one-path, two-path and three-path reference signals, the measurement results are shown as the green, cyan and red curves, respectively. It can be observed that the depth of cancellation does not decrease significantly when the number of SRs is insufficient. This is mainly caused by the interaction between the residual interfering signal and the reference signal. Then, when the three-path SI signals are cancelled simultaneously, the depth of cancellation at the corresponding frequency points reaches 48.9, 47.8, 47.5, and 45.9 dB, respectively. For the single-frequency single-path SIC, the simulation results show that the theoretical cancellation depth does not exceed 33.5 dB when the phase deviation between the reference signal and the interfering signal is 1.0° and the amplitude deviation is 0.1 dB [33]. Hence, according to the single-frequency SIC simulation results, it can be inferred that the experimental system has a high accuracy of phase and amplitude adjustment.

Next, a linear frequency modulation (LFM) signal was used as the transmitting signal to verify the broadband multipath cancellation ability of the system. In order to demonstrate the cancellation effect more intuitively, a single-frequency signal was used as the SOI signal in this experiment. The MSG was set to output LFM signals with centre frequencies of 4, 6, 8 and 10 GHz, with bandwidths the same as 100 MHz. The spectra were measured as shown in Fig. 7. For the one-path, two-path and three-path reference signals, the measurement results are shown as the green, cyan and red curves, respectively. From the blue curves, it can be seen that the SOI signals are completely submerged by the SI signals. One-path and two-path cancellations were then implemented. It was found that the three-path SI signal was effectively suppressed when there were not enough reference signals as a match. In addition to the interference from the residual SI signal, the non-uniformity in the frequency response of the system also caused depressions and lifts in the spectra. When three reference signals were applied for cancellation, the cancellation depths of the LFM signals with centre frequencies of 4, 6, 8 and 10 GHz were 32.7, 26.1, 28.5 and 23.9 dB, respectively.

Finally, the recovery of the vector signal under three SI paths was experimentally verified. A vector signal generator (VSG, Keysight, N5182B) was used to generate an SOI signal with a centre frequency of 6 GHz, a modulation format of 16 QAM, and a code rate of 10 Mbps. The SI signal was a LFM signal with a bandwidth of 20 MHz. The blue curve in Fig. 8(a) and (b) show the spectrum and constellation diagram for the received signal when the multipath SIC was not used. It can be seen that the received signal is severely distorted and cannot be demodulated. As shown in Fig. 8(c) and (d), after one-path and two-path cancellation, the EVM values are still greater than the 13.5% threshold mandated by the 3GPP protocol. The spectrum after multipath SIC is shown as the red curve in Fig. 8(a), and the constellation diagram after multipath SIC is shown in Fig. 8(e). The constellation diagram is much clearer, meaning that the multipath SI signals have been effectively suppressed. The error vector magnitude (EVM) is reduced from 22.4% to 8.9%, which satisfies the requirements for the 3GPP protocol for the demodulation of 16QAM signals.

Various SIC methods are compared in Table 1. Reference [17] can only realize a single-path cancellation, rather than multi-path cancellation. In reference [9], the time delay is controlled by a dispersion element, and the SIC depth is quite fine. However, higher requirements have been put forward for tunable lasers, including tuning accuracy and the range. In reference [20], the number of multiple lasers and PMs increases with the number of cancellation paths, which constrains system scalability. Meanwhile, since an optical filter is applied to extract one of the RF sidebands produced by the PMs, the low operation frequency of SI is limited. Similarly, multiple lasers are also required to form

TABLE 1
COMPARISON OF VARIOUS SIC SCHEMES

Methods	Number of lasers	Lower Operation frequency (GHz)	Number of SI	Bandwidth (GHz)	SIC depth (dB)	Expansion cost
Proposed method	1	Not limited	3	0.1	23.9	low
Dispersive Element [9]	N+1	Not limited	2	0.05	44	high
Dual MZM [17]	2	Not limited	1	0.096	33	Unable
Phase modulator [20]	N+1	Limited	2	0.1	26	high
Dual MZM+DWDM [21]	N+1	Not limited	3	2	20.88	middle
SM-MM [22]	2	Not limited	2	0.2	35	high

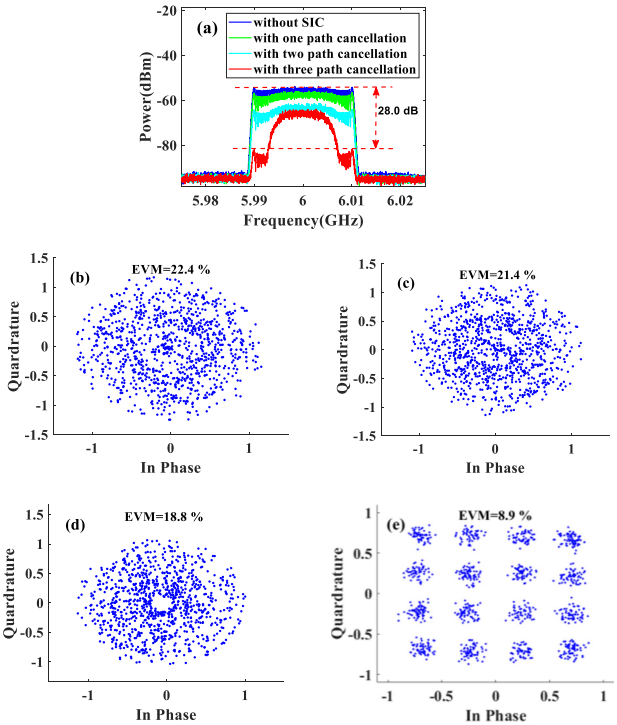

Fig. 8. (a) Spectra before and after cancellation; (b)–(e) constellation diagram with no SIC, one-path cancellation, two-path cancellation, and three-path cancellation.

several incoherent SR paths for multi-path SIC in [21], so the system cost and complexity are high. Reference [22] reduces the number of lasers through an SM-MM coupler, however, this coupler can only supply limited incoherent SR signals. In the proposed method, a single laser is applied to generate OFC through the RFS loop. Except the original optical carrier, other combs can be applied as multiple incoherent SR optical signals, avoiding the usage of multiple lasers. On the one hand, a large number of incoherent SR optical signals can be produced, making this method highly scalable and more suitable for complex practical applications that require multiple incoherent SR paths. Additionally, the number of SR optical signals in the OFC can be easily controlled by adjusting the bandwidth of the OCF in the RFS loop, making the system more flexible and more compact compared to other multi-laser schemes.

IV. CONCLUSION

An optical-domain multipath self-interference cancellation method based on RFS-OFC was theoretically and experimentally verified for multipath SIC. An RFS-OFC based on CS-SSB modulation was introduced to the multipath SIC, which was used to provide reference optical signals. This structure is more flexible and compact than other multi-laser schemes, and no special devices are required to remove coherence between multiple reference signals compared to other single-laser methods. The RF signals were phase-inverted by dual MZMs working at opposite quadrature bias points. The amplitude and delay matching were realised by sets of VOLs and OTDLs rather than electrical devices. For a situation with three SI paths, the experimental results showed that the system had a single frequency and a wideband cancellation depth of more than 45.9 dB and 23.9 dB, respectively. The 16QAM signal could be recovered with an excellent constellation diagram. The EVM of this signal was improved from 22.4% to 8.9%. Full optical domain regulation of the delay, phase and amplitude is beneficial in terms of an increase in the bandwidth and the operating frequency of the SIC system. By adjusting the bandwidth of the bandpass filter in RFS, the number of optical carriers can easily be raised, meaning that the system has good scalability and flexibility for practical complex scenarios with more SI paths.

REFERENCES

[1] C. Cox and E. Ackerman, "Microwave photonics: Past, present and future," in *Proc. Int. Topical Meeting Microw. Photon. Jointly Held Asia-Pacific Microw. Photon. Conf.*, 2008, pp. 9–11.
[2] R. A. Minasian, E. H. Chan, and X. Yi, "Microwave photonic signal processing," *Opt. Exp.*, vol. 21, no. 19, pp. 22918–22936, 2013.
[3] S. Pan and J. Yao, "Photonics-based broadband microwave measurement," *J. Lightw. Technol.*, vol. 35, no. 16, pp. 3498–3513, Aug. 2017.
[4] X. Han et al., "RF self-interference cancellation by using photonic technology," *Chin. Opt. Lett.*, vol. 19, no. 7, 2021, Art. no. 073901.
[5] N. Shi, Q. Song, J. Tang, W. Li, N. Zhu, and M. Li, "A switchable selfinterference cancellation system for dual-band IBFD system using a monolithic integrated DML array," *Opt. Commun.*, vol. 447, pp. 55–60, 2019.
[6] F. Shen et al., "Simulation and performance analysis of photonic integrated RF self-interference cancellation system," *Acta Photon. Sinica*, vol. 48, 2019, Art. no. 1148017.
[7] K. E. Kolodziej, S. Yegnanarayanan, and B. T. Perry, "Photonic-enabled RF canceller for wideband in-band full-duplex wireless systems," *IEEE Trans. Microw. Theory Techn.*, vol. 67, no. 5, pp. 2076–2086, May 2019.
[8] K. E. Kolodziej, S. Yegnanarayanan, and B. T. Perry, "Fiber Bragg grating delay lines for wideband self-interference cancellation," *IEEE Trans. Microw. Theory Techn.*, vol. 67, no. 10, pp. 4005–4014, Oct. 2019.
[9] W. Zhou, P. Xiang, Z. Niu, M. Wang, and S. Pan, "Wideband optical multipath interference cancellation based on a dispersive element," *IEEE Photon. Technol. Lett.*, vol. 28, no. 8, pp. 849–851, Apr. 2016.
[10] Y. Xiang, G. Li, and S. Pan, "Ultrawideband optical cancellation of RF interference with phase change," *Opt. Exp.*, vol. 25, no. 18, pp. 21259–21264, 2017.

[11] M. P. Chang, C.-L. Lee, B. Wu, and P. R. Prucnal, "Adaptive optical selfinterference cancellation using a semiconductor optical amplifier," *IEEE Photon. Technol. Lett.*, vol. 27, no. 9, pp. 1018–1021, May 2015.

[12] B. Weng, M. Chang, and Y. Chen, "Radio-frequency self-interference cancellation using a dual-drive Mach-Zehnder modulator and a fiber Bragg grating," *Opt. Eng.*, vol. 57, no. 8, 2018, Art. no. 083107.

[13] S. Zhang, S. Xiao, Y. Zhang, H. Feng, L. Zhang, and Z. Zhou, "Directly modulated laser-based optical radio frequency self-interference cancellation system," *Opt. Eng.*, vol. 55, no. 2, 2016, Art. no. 026116.

[14] J. Wang, Y. Wang, Z. Zhang, Z. Zhao, and J. Liu, "Optical self-interference cancellation with frenquency down-conversion based on cascade modulator," *IEEE Photon. J.*, vol. 12, no. 6, Dec. 2020, Art. no. 5502708.

[15] Q. Zhou, H. Feng, G. Scott, and M. Fok, "Wideband co-site interference cancellation based on hybrid electrical and optical techniques," *Opt. Lett.*, vol. 39, no. 22, pp. 6537–6540, 2014.

[16] X. Han, B. Huo, Y. Shao, C. Wang, and M. Zhao, "RF self-interference cancellation using phase modulation and optical sideband filtering," *IEEE Photon. Technol. Lett.*, vol. 29, no. 11, pp. 917–920, Jun. 2017.

[17] J. Suarez, K. Kravtsov, and P. R. Prucnal, "Incoherent method of optical interference cancellation for radio-frequency communications," *IEEE J. Quantum Electron.*, vol. 45, no. 4, pp. 402–408, Apr. 2009.

[18] X. Han, B. Huo, Y. Shao, and M. Zhao, "Optical RF self-interference cancellation by using an integrated dual-parallel MZM," *IEEE Photon. J.*, vol. 9, no. 2, Apr. 2017, Art. no. 5501308.

[19] M. Huang, D. Zhu, and S. Pan, "Optical RF interference cancellation based on a dual-parallel polarization modulator," in *Proc. Asia Commun. Photon. Conf.*, 2014, Paper ATh1F.6.

[20] X. Su et al., "Optical multipath RF self-interference cancellation based on phase modulation for full-duplex communication," *IEEE Photon. J.*, vol. 12, no. 4, Aug. 2020, Art. no. 7102114.

[21] X. Yu, J. Ye, L. Yan, T. Zhou, X. Zou, and W. Pan, "Photonic-assisted multipath self-interference cancellation for wideband MIMO radio over-fiber transmission," *J. Lightw. Technol.*, vol. 40, no. 2, pp. 462–469, Jan. 2022.

[22] J. Chang and P. R. Prucnal, "A novel analog photonic method for broadband multipath interference cancellation," *IEEE Microw. Wireless Compon. Lett.*, vol. 23, no. 7, pp. 377–379, Jul. 2013.

[23] M. P. Fok, Y. Deng, K. Kravtsov, and P. R. Prucnal, "Signal beating elimination using single-mode fiber to multimode fiber coupling," *Opt. Lett.*, vol. 36, no. 23, pp. 4578–4580, 2011.

[24] D. Chapman, "Low-loss many-to-one fiber couplers with few or single-mode inputs and a multi-mode output," *Fiber Integr. Opt.*, vol. 23, no. 5, pp. 375–385, 2004.

[25] Y. Zhang et al., "EML-based multi-path self-interference cancellation with adaptive frequency-domain pre-equalization," *IEEE Photon. Technol. Lett.*, vol. 30, no. 12, pp. 1103–1106, Jun. 2018.

[26] X. Li et al., "Optimized self-interference cancellation based on optical dual-parallel MZM for co-frequency and co-time full duplex wireless communication under nonlinear distortion and emulated multipath effect," *Opt. Exp.*, vol. 27, no. 26, pp. 37286–37297, 2019.

[27] M. Han, T. Shi, and Y. Chen, "Digital-assisted photonic analog wideband multipath self-interference cancellation," *IEEE Photon. Technol. Lett.*, vol. 34, no. 5, pp. 299–302, Mar. 2022.

[28] L. Zheng, Z. Liu, S. Xiao, M. Fok, Z. Zhang, and W. Hu, "Hybrid wideband multipath self-interference cancellation with an LMS pre-adaptive filter for in-band full-duplex OFDM signal transmission," *Opt. Lett.*, vol. 45, no. 23, pp. 6382–6385, 2020.

[29] S. Diddams, "The evolving optical frequency comb," *Opt. Lett.*, vol. 27, no. 11, pp. B51–B62, 2010.

[30] S. Han, Y. Kim, and S. Kim, "Parallel determination of absolute distances to multiple targets by time-of-flight measurement using femtosecond light pulses," *Opt. Exp.*, vol. 23, no. 20, pp. 25874–25882, 2015.

[31] Z. Tang, D. Zhu, and S. Pan, "Coherent optical RF channelizer with large instantaneous bandwidth and large in-band interference suppression," *J. Lightw. Technol.*, vol. 36, no. 19, pp. 4219–4226, Oct. 2018.

[32] W. Chen, D. Zhu, C. Xie, and J. Liu, "Microwave channelizer based on a photonic dual-output image-reject mixer," *Opt. Lett.*, vol. 44, no. 16, pp. 4052–4055, 2019.

[33] X. Fang, M. Bai, X. Ye, J. Miao, and Z. Zheng, "Ultra-broadband microwave frequency down-conversion based on optical frequency comb," *Opt. Exp.*, vol. 23, no. 13, pp. 17111–17119, 2015.

[34] H. Jung, C. Xiong, K. Fong, X. Zhang, and H. Tang, "Optical frequency comb generation from aluminum nitride microring resonator," *Opt. Lett.*, vol. 38, no. 15, pp. 2810–2813, 2013.

[35] J. S. Parker, A. Bhardwaj, P. R. A. Binetti, Y.-J. Hung, and L. A. Coldren, "Monolithically integrated gain-flattened ring mode-locked laser for comb-line generation," *IEEE Photon. Technol. Lett.*, vol. 24, no. 2, pp. 131–133, Jan. 2012.

[36] Q. Wang, L. Huo, Y. Xing, and B. Zhou, "Ultra-flat optical frequency comb generator using a single-driven dual-parallel Mach–Zehnder modulator," *Opt. Lett.*, vol. 39, no. 10, pp. 3050–3053, 2014.

[37] Y. Liu et al., "Bandwidth scaling of a phase-modulated continuous-wave comb through four-wave mixing in a silicon nano-waveguide," *Opt. Lett.*, vol. 39, no. 22, pp. 6478–6481, 2014.

[38] J. Li, X. Zhang, F. Tian, and L. Xi, "Theoretical and experimental study on generation of stable and high-quality multicarrier source based on recirculating frequency shifter used for Tb/s optical transmission," *Opt. Exp.*, vol. 19, no. 2, pp. 848–860, 2011.

[39] J. Lin, L. Xi, J. Li, X. Zhang, X. Zhang, and S. A. Niazi, "Low noise optical multi-carrier generation using optical-FIR filter for ASE noise suppression in re-circulating frequency shifter loop," *Opt. Exp.*, vol. 22, no. 7, pp. 7852–7864, 2014.